

Notes on TERS theory — Part I

by Dr. Sergey A. Saunin and Dr. Michael A. Trusov,
AIST-NT Co., Moscow, Zelenograd*

Abstract

The first part of the notes concerns the basic results of electromagnetic field intensity enhancement calculation between probe and wafer in the electrostatic limit.

1 Introduction

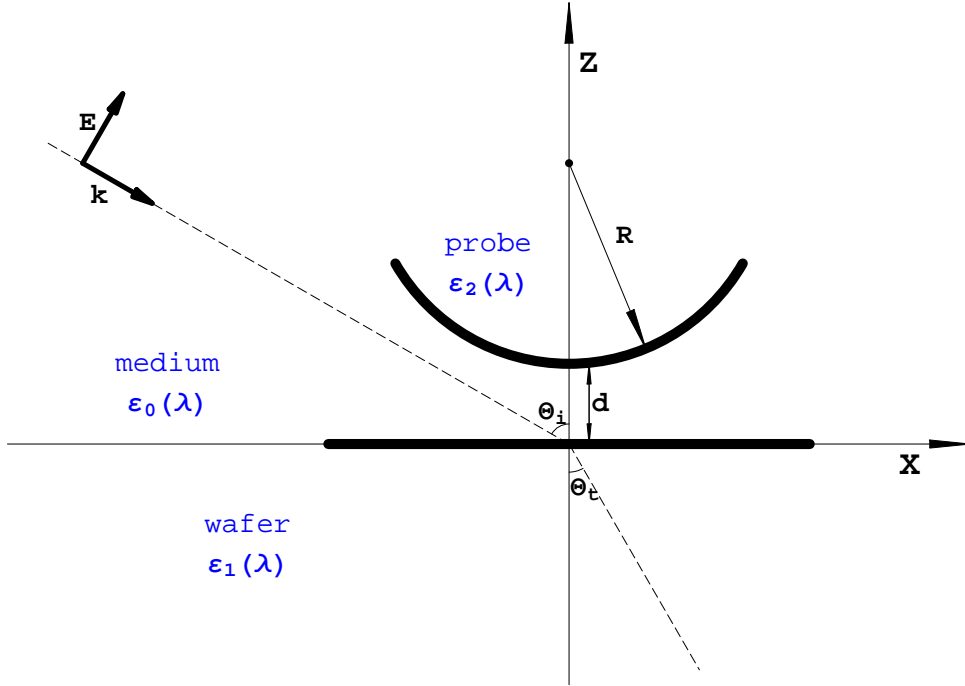
Now it is well known that electromagnetic field concentration and amplification between probe and wafer is a crucial factor to observe tip-enhanced Raman scattering phenomena. The value of the field intensity enhancement can be in principal calculated by numerical solving of Maxwell equations together with proper boundary conditions. However, such a numerical simulation requires substantial computational resources and does not allow to study immediately the dependence of the field intensity distribution on the system geometry and configuration.

In these notes we present the results of an approximate calculation using some simplifying assumptions. Although the calculation precision is not very high, this approach allows one to estimate quite fast the enhancement at least up to the order of magnitude, to obtain the field intensity as a function of system parameters, and to determine what crucial points prove very important in the system design and construction.

Let us consider an electromagnetic wave propagation in the homogeneous medium (e.g., air) above a smooth horizontal metallic wafer (which we take into account as a homogeneous half-space) in presence of the metallic probe located near the wafer (see Fig. 1). We describe the probe, wafer and medium materials via their complex dielectric permittivities (*first simplification*), so the system of Maxwell equation reduces to the system of

*website: <http://www.aist-nt.com/>

Figure 1: The geometry of the system: a planar P-polarized wave with wavelength λ and wave-vector \mathbf{k} propagating through the medium with permittivity $\varepsilon_0(\lambda)$ falls onto a plane surface of the metallic wafer with permittivity $\varepsilon_1(\lambda)$. A metallic probe with permittivity $\varepsilon_2(\lambda)$ is embedded inside the medium close to wafer at a distance d , and we are interested in the electromagnetic field intensity distribution near the probe tip.



Helmholtz equations on the electric field components for each of three corresponding space regions.

Suppose now that both the radius of curvature of the probe tip and the distance between probe and wafer are much less than incident wavelength. Then, as we are interested in the field distribution close to the probe tip, we may consider the problem in the electrostatic limit (*second simplification*) and reduce the Helmholtz equations to the Laplace equations much easier to solve.

Following this program, in the second section we adduce explicit expressions for the field components and the field intensity near the probe tip in the electrostatic limit. The results are based on formulas quoted in papers [1]–[6]. In the third section we show figures clearly demonstrating the possibility of enormous field amplification and discuss the necessary conditions to reach it. Finally, the fourth section is a short conclusion.

2 Field computation

The configuration of the system under investigation is shown on Fig. 1 (for P-polarized case). A planar wave with wavelength λ and wave-vector \mathbf{k} propagating through the medium with permittivity $\varepsilon_0(\lambda)$ falls onto a plane surface of the metallic wafer with permittivity $\varepsilon_1(\lambda)$. A metallic probe with permittivity $\varepsilon_2(\lambda)$ is embedded inside the medium close to wafer at a distance d , the probe tip curvature radius is R . The wave incident angle is Θ_i , the refraction angle is Θ_t ; those being related via Snell's law:

$$\frac{\sin \Theta_i}{\sin \Theta_t} = \sqrt{\frac{\varepsilon_1}{\varepsilon_0}}.$$

Suppose the incident wave being polarized and expand the initial electric field \mathbf{E}_i of the wave onto S-component $E_i^{(S)}$ and P-component $E_i^{(P)}$. In absence of the probe the fields \mathbf{E}_u and \mathbf{E}_d above and under the boundary surface are described by Fresnel formulas¹:

$$\begin{aligned} E_u^{(x)} &= E_d^{(x)} = E_i^{(P)} \cdot \frac{2 \cos \Theta_i \cos \Theta_t}{\cos \Theta_t + \sqrt{\varepsilon_1} \cos \Theta_i}, \\ E_u^{(y)} &= E_d^{(y)} = E_i^{(S)} \cdot \frac{2 \cos \Theta_i}{\cos \Theta_i + \sqrt{\varepsilon_1} \cos \Theta_t}, \\ E_u^{(z)} &= \varepsilon_1 E_d^{(z)} = E_i^{(P)} \cdot \frac{2 \varepsilon_1 \cos \Theta_i \sin \Theta_t}{\cos \Theta_t + \sqrt{\varepsilon_1} \cos \Theta_i}, \end{aligned}$$

so that the field intensity distribution along the wafer surface is uniform. But the presence of the probe redistribute the field energy density collecting most of it under the probe tip.

Assuming (in view of the aforesaid) the condition $d, R \ll \lambda$, we consider the problem in the electrostatic limit. The electric field inside the medium (\mathbf{E}_0), wafer (\mathbf{E}_1) and probe (\mathbf{E}_2) can be expressed via corresponding potentials Φ_0 , Φ_1 , and Φ_2 as follows:

$$\mathbf{E}_0 = -\nabla \Phi_0, \quad \mathbf{E}_1 = -\nabla \Phi_1, \quad \mathbf{E}_2 = -\nabla \Phi_2.$$

The potentials satisfy the equations

$$\Delta \Phi_0 = \Delta \Phi_1 = \Delta \Phi_2 = 0$$

¹In what follows for simplicity we put $\varepsilon_0(\lambda) \equiv 1$; the generalization to the case $\varepsilon_0 \neq 1$ is obvious.

and boundary conditions

$$\begin{aligned}\Phi_0 &= \Phi_1, & \frac{\partial}{\partial n}\Phi_0 &= \varepsilon_1 \frac{\partial}{\partial n}\Phi_1 & \text{at wafer surface,} \\ \Phi_0 &= \Phi_2, & \frac{\partial}{\partial n}\Phi_0 &= \varepsilon_2 \frac{\partial}{\partial n}\Phi_2 & \text{at probe surface,} \\ \Phi_0 &\sim -\mathbf{E}_u \mathbf{r}, & \Phi_1 &\sim -\mathbf{E}_d \mathbf{r} & \text{at } r \rightarrow \infty.\end{aligned}$$

To step further, it is convenient to introduce the bispherical coordinates σ, τ, φ instead of Cartesian X,Y,Z

$$\begin{aligned}X &= \rho \cos \phi, & Y &= \rho \sin \phi, & \rho &= \sqrt{X^2 + Y^2}, \\ \rho &= a \frac{\sin \sigma}{\cosh \tau - \cos \sigma}, & Z &= a \frac{\sinh \tau}{\cosh \tau - \cos \sigma}, \\ \tau &= \frac{1}{2} \ln \frac{\rho^2 + (z+a)^2}{\rho^2 + (z-a)^2}, & \sigma &= \arccos \frac{\rho^2 + z^2 - a^2}{[(\rho^2 + (z+a)^2)(\rho^2 + (z-a)^2)]^{1/2}}, \\ & & & & -\infty < \tau < +\infty, & 0 \leq \phi < 2\pi, & 0 \leq \sigma \leq \pi,\end{aligned}$$

where $a = \sqrt{d^2 - R^2}$. Note, the surface $\tau = 0$ corresponds to the wafer boundary, while the surface

$$\tau = \tau_0 \stackrel{\text{def}}{=} \log \frac{d+a}{R}$$

corresponds to the probe boundary.

Now the local amplification of the field intensity at a given point can be expressed via Φ_0 function as follows:

$$\frac{I}{I_0} = \frac{(\cosh \tau - \cos \sigma)^2}{a^2} \cdot \frac{|\partial_\tau \Phi_0|^2 + |\partial_\sigma \Phi_0|^2 + \frac{1}{\sin^2 \sigma} |\partial_\varphi \Phi_0|^2}{|E_i^{(P)}|^2 + |E_i^{(S)}|^2},$$

and the remaining question is: how to calculate the Φ_0 function?

Omitting intermediate calculations let us present here only the final result. The function Φ_0 can be written as combination of two Fourier series:

$$\begin{aligned}\Phi_0 &= \left(-\rho + \sqrt{\cosh \tau - \cos \sigma} F_0^\rho \right) \left(E_u^{(x)} \cos \varphi + E_u^{(y)} \sin \varphi \right) \\ &\quad + \left(-z + \sqrt{\cosh \tau - \cos \sigma} F_0^z \right) E_u^{(z)}\end{aligned}$$

where

$$F_0^\rho = \sum_{n=1}^{\infty} A_n^\rho P_n^1(\cos \sigma) \left(e^{(n+\frac{1}{2})\tau} + \frac{1-\varepsilon_1}{1+\varepsilon_1} e^{-(n+\frac{1}{2})\tau} \right)$$

$$F_0^z = \sum_{n=1}^{\infty} A_n^z P_n(\cos \sigma) \left(e^{(n+\frac{1}{2})\tau} + \frac{1-\varepsilon_1}{1+\varepsilon_1} e^{-(n+\frac{1}{2})\tau} \right)$$

Here $P_n(\cos \sigma)$ is the ordinary Legendre polynomial, while $P_n^1(\cos \sigma)$ is the adjoint Legendre function:

$$P_n^1(\cos \sigma) = -\sin \sigma P_n'(\cos \sigma).$$

To determine the expansion coefficients one should solve the band system of linear equations for A_n^ρ

$$(n-1) \left(\frac{1-\varepsilon_1}{1+\varepsilon_1} e^{-2n\tau_0} - \frac{1+\varepsilon_2}{1-\varepsilon_2} e^{-\tau_0} \right) \cdot A_{n-1}^\rho$$

$$+ \left[\left(1 + \frac{1-\varepsilon_1}{1+\varepsilon_1} e^{-(2n+1)\tau_0} \right) \sinh \tau_0 \right.$$

$$+ \left. (2n+1) \left(\frac{1+\varepsilon_2}{1-\varepsilon_2} - \frac{1-\varepsilon_1}{1+\varepsilon_1} e^{-(2n+1)\tau_0} \right) \cosh \tau_0 \right] \cdot A_n^\rho$$

$$+ (n+2) \left(\frac{1-\varepsilon_1}{1+\varepsilon_1} e^{-(2n+2)\tau_0} - \frac{1+\varepsilon_2}{1-\varepsilon_2} e^{\tau_0} \right) \cdot A_{n+1}^\rho$$

$$= 4\sqrt{2}a \sinh \tau_0 e^{-(2n+1)\tau_0},$$

$$A_0^\rho \equiv 0, \quad n = 1, 2, \dots,$$

and analogously for A_n^z

$$n \left(\frac{1-\varepsilon_1}{1+\varepsilon_1} e^{-2n\tau_0} - \frac{1+\varepsilon_2}{1-\varepsilon_2} e^{-\tau_0} \right) \cdot A_{n-1}^z$$

$$+ \left[\left(1 + \frac{1-\varepsilon_1}{1+\varepsilon_1} e^{-(2n+1)\tau_0} \right) \sinh \tau_0 \right.$$

$$+ \left. (2n+1) \left(\frac{1+\varepsilon_2}{1-\varepsilon_2} - \frac{1-\varepsilon_1}{1+\varepsilon_1} e^{-(2n+1)\tau_0} \right) \cosh \tau_0 \right] \cdot A_n^z$$

$$+ (n+1) \left(\frac{1-\varepsilon_1}{1+\varepsilon_1} e^{-(2n+2)\tau_0} - \frac{1+\varepsilon_2}{1-\varepsilon_2} e^{\tau_0} \right) \cdot A_{n+1}^z$$

$$= 2\sqrt{2}a (\cosh \tau_0 - (2n+1) \sinh \tau_0) e^{-(2n+1)\tau_0},$$

$$A_{-1}^z \equiv 0, \quad n = 0, 1, \dots$$

Note the linear system for $A_n^{\rho,z}$ is three-diagonal, which allows to solve it quite fast using well-known linear algebra tools. To check the series convergence one may use the “sum rule”

$$\sum_{n=0}^{\infty} A_n^z = 0,$$

being a consequence from the Gauss law

$$\oint \mathbf{E}_0 \cdot d\mathbf{S} = 0.$$

3 Results and discussion

After deriving explicit formulas for the electromagnetic field intensity one may investigate its dependence on the observation point, on the system geometry and on the incident light wavelength. As an example, we have taken for analysis the following system: silver probe, gold wafer, and air medium, have fixed the incident angle $\theta_i = 45^\circ$ and the P-polarization of the incident light (except for the item 2), and have made the following numerical simulations:

- 1) First of all we fix parameters $d=3$ nm, $R=100$ nm and study the field distribution in the XYZ space near the probe tip. The intensity dependence on the Z coordinate directly under the probe ($X=0$ nm, $Y=0$ nm) is very weak which is illustrated on Fig. 2. The intensity dependence on the X coordinate at $Y=0$ nm, $Z=1$ nm is presented on Fig. 3 while the intensity 2D distribution at $Z=1$ nm is presented on Fig. 4, both for wavelengths **653 nm** and **775 nm**. One can see explicitly the characteristic resonance behaviour on Fig. 3 with damping length $\ell \approx \sqrt{2dR} \approx 25$ nm (this formula works quite well for the case $d \ll R \ll \lambda$), and the geometrically shadowed region on the right-hand side of the probe on Fig. 4.
- 2) Then we fix parameters $d=3$ nm, $R=100$ nm, the observation point $X=0$ nm, $Y=0$ nm, $Z=1$ nm and study the field intensity behaviour under the incident light polarization rotation for wavelengths **653 nm** and **775 nm**. The result is presented on Fig. 5. One can see the strong intensity reduction on changing the P-polarization to S-polarization.
- 3) Then we fix parameter $R=100$ nm, the observation point $X=0$ nm, $Y=0$ nm, and study the field intensity directly on the probe tip as a function of the probe-wafer distance d for wavelengths **653 nm** and **775 nm**.

Figure 2: Local field intensity dependence on the observation point directly under the probe tip (logarithmic scale). Here $R=100$ nm, $d=3$ nm, $X=0$ nm, $Y=0$ nm; incident light wavelength: 653 nm and 775 nm.

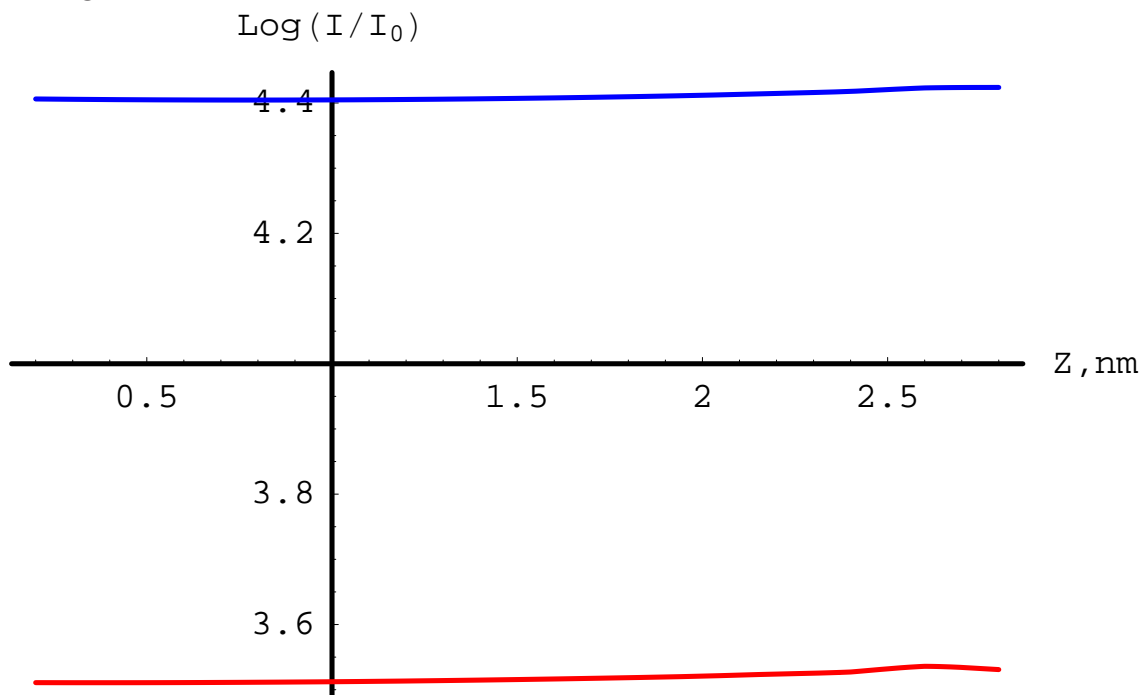


Figure 3: Local field intensity dependence on the observation point (1D-plot, logarithmic scale). Here $R=100$ nm, $d=3$ nm, $Y=0$ nm, $Z=1$ nm; incident light wavelength: 653 nm and 775 nm. Resonance damping length $\ell \approx 25$ nm.

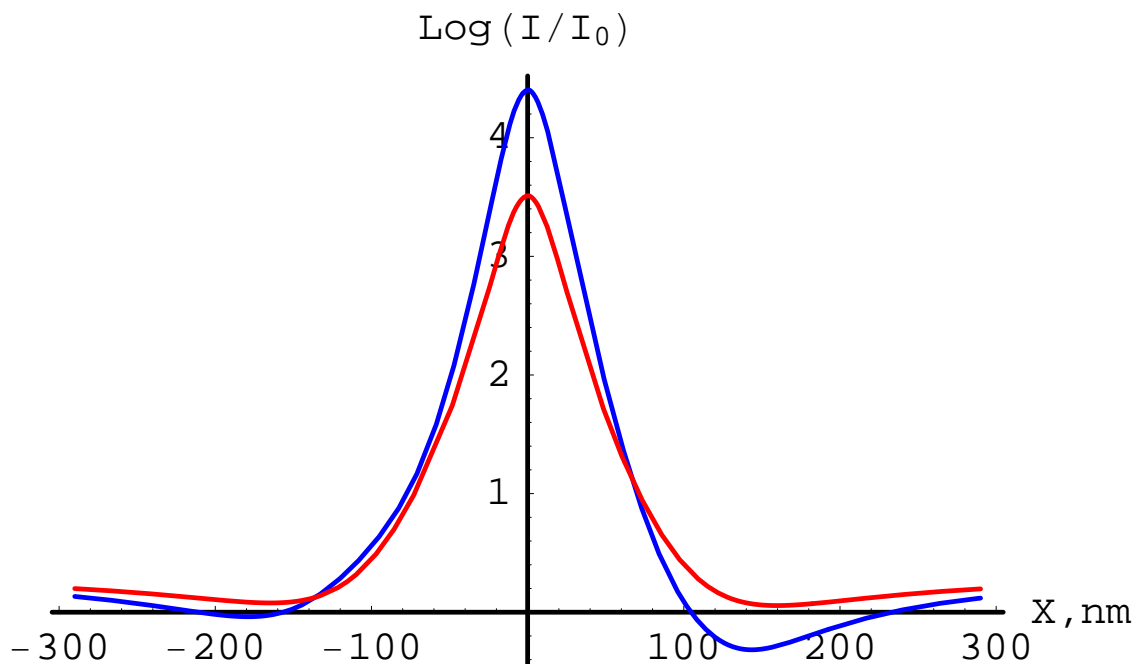


Figure 4: Local field intensity dependence on the observation point (2D-plot, logarithmic scale). Here $R=100$ nm, $d=3$ nm, $Z=1$ nm; incident light wavelength: 653 nm and 775 nm.

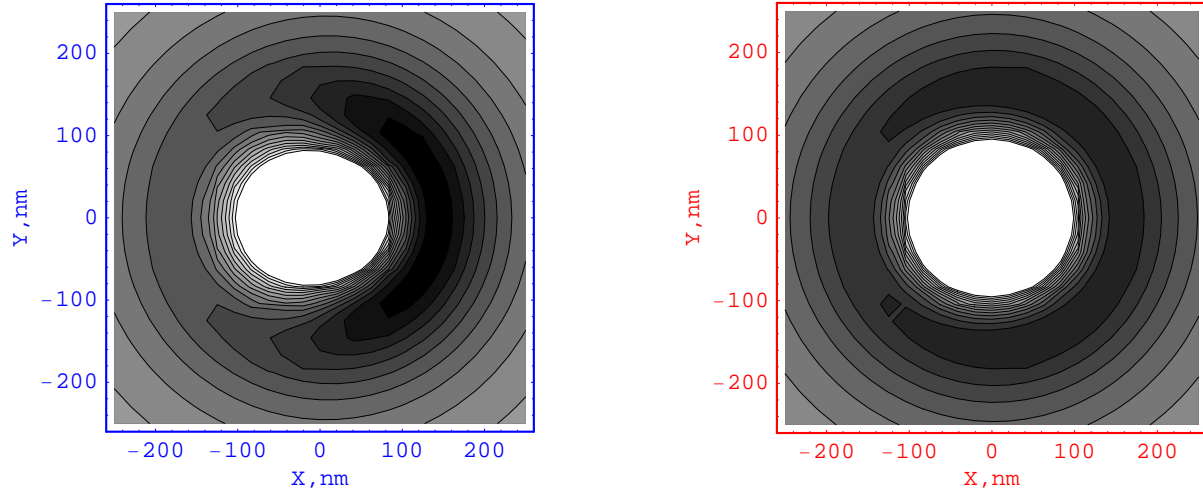


Figure 5: Local field intensity reduction (logarithmic scale) at the incident light polarization rotation from P ($\varphi = 0$) to S ($\varphi = \pm 90$). Here $R=100$ nm, $d=3$ nm, $X=0$ nm, $Y=0$ nm, $Z=1$ nm; incident light wavelength: 653 nm and 775 nm.

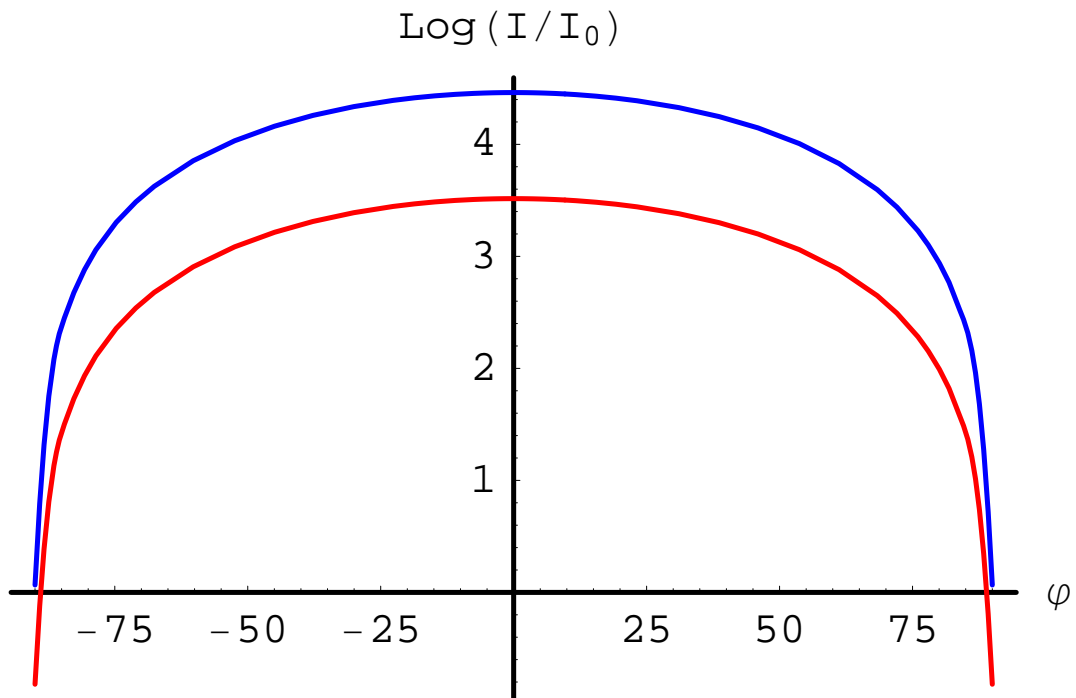
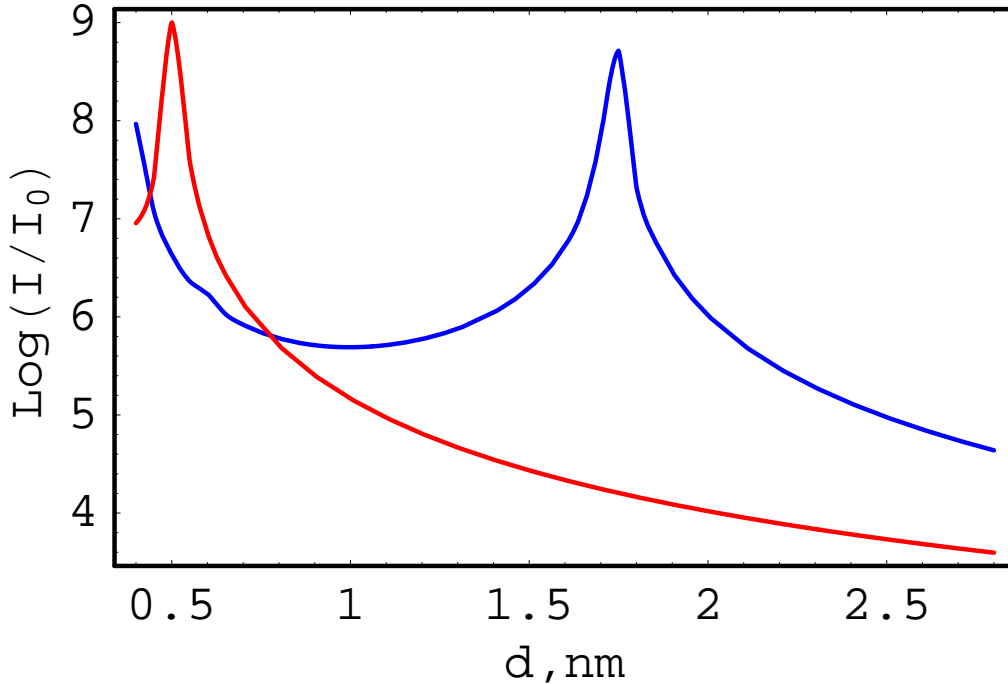


Figure 6: Local field intensity dependence (logarithmic scale) on the probe-wafer distance d . Here $R=100$ nm, $X=0$ nm, $Y=0$ nm; incident light wavelength: 653 nm and 775 nm.



The result is presented on Fig. 6. One can see high field amplification for the resonance distances determined by the Malshukov formula for “gap modes” (see [5]):

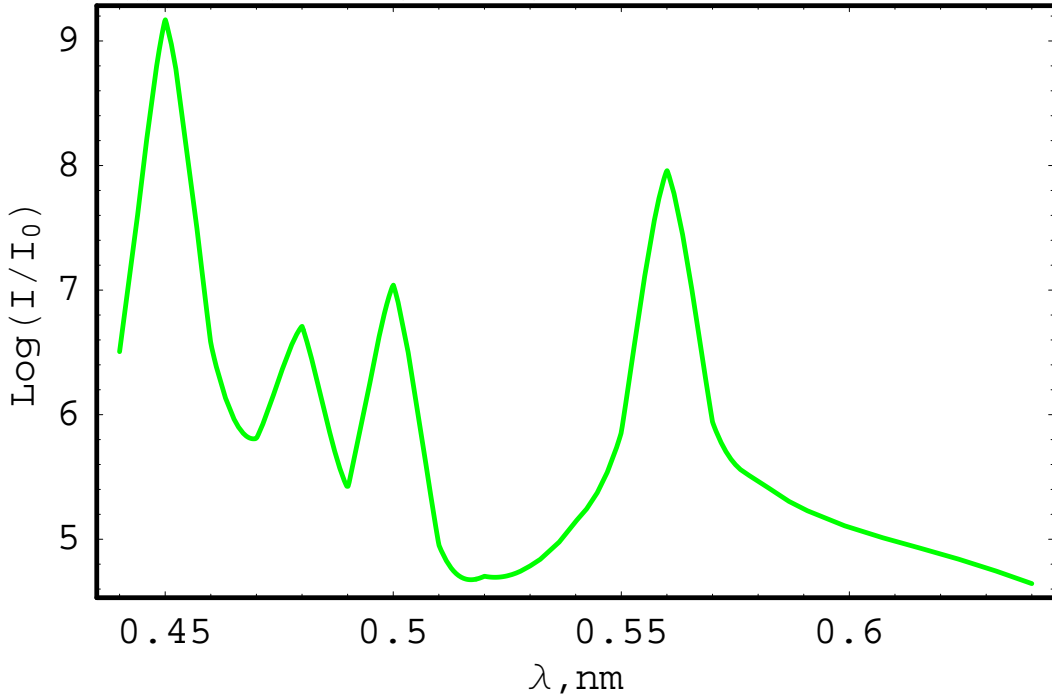
$$d_{\text{res}} \approx 2R \left(\frac{1}{\text{Re} \varepsilon_{\text{Au}}(\lambda)} + \frac{1}{\text{Re} \varepsilon_{\text{Ag}}(\lambda)} \right)^2$$

4) Finally we fix parameters $d=3$ nm, $R=100$ nm, the observation point $X=0$ nm, $Y=0$ nm, $Z=1$ nm and study the field intensity behaviour under the incident light wavelength λ . The result is presented on Fig. 7. The dependence is extremely irregular (which caused, most of all, by an irregular behaviour of functions $\varepsilon_{\text{Au}}(\lambda)$ and $\varepsilon_{\text{Ag}}(\lambda)$), and one can see that to provide the high field intensity amplification the incident light wavelength should be tuned much accurately.

4 Conclusions

In the electrostatic limit using the approximation of homogeneous mediums we have calculated the electromagnetic field intensity distribution in the probe-wafer configuration. Our analysis shows that the local field intensity enhancement under the probe tip can be 10^8 or higher at the

Figure 7: Local field intensity dependence (logarithmic scale) on the light wavelength λ . Here $R=100$ nm, $d=3$ nm, $X=0$ nm, $Y=0$ nm, $Z=1$ nm.



resonance point, which allows one to obtain good Raman signal from very small specimens, up to a single molecule.

We have shown that to obtain high signal amplification one should fit accurately the incident light wavelength or/and the probe-wafer distance, both being strongly dependent on probe and wafer materials and system geometrical parameters. Also it is quite important to provide the excitation light polarization being parallel to the plane of incidence (P-polarization).

References

- [1] R.W.Rendell, D.J.Scalapino, and B.Mühlschlegel, “*Role of local plasmon modes in light emission from small-particle tunnel junctions*”, Physical Review Letters, vol. 41, pp. 1746-1750 (1978).
- [2] R.W.Rendell and D.J.Scalapino, “*Surface plasmon confined by microstructures on tunnel junctions*”, Physical Review B, vol. 24, pp. 3276-3294 (1981).
- [3] P.K.Aravind and H.Metiu, “*The effects of the interaction between resonances in the electromagnetic response of a sphere-plane structure;*

applications to surface enhanced spectroscopy”, Surface Science, vol. 124, pp. 506-528 (1983).

- [4] G.T.Boyd, Th.Rasing, J.R.R.Leite, and Y.R.Shen, “*Local-field enhancement on rough surfaces of metals, semimetals, and semiconductors with the use of optical second-harmonic generation*”, Physical Review B, vol. 30, pp. 519-526 (1984).
- [5] A.G.Malshukov, “*Surface enhances Raman scattering: the present status*”, Physics Reports, vol. 194, pp. 343-349 (1990).
- [6] V.N.Konopsky, S.A.Saunin, V.A.Bykov, and E.A.Vinogradov, “*Scanning plasmon near-field microscopy: signal-noise ratio of different registration schemes and prospects for single molecule detection*”, Physical Chemistry and Chemical Physics, vol. 4, pp. 2733-2737 (2002).